

RESEARCH

Open Access



# Investigation in the cannabigerol derivative VCE-003.2 as a disease-modifying agent in a mouse model of experimental synucleinopathy

Sonia Burgaz<sup>1,2,3</sup>, Elisa Navarro<sup>1,2,3</sup>, Santiago Rodríguez-Carreiro<sup>1,2,3</sup>, Carmen Navarrete<sup>4</sup>, Martin Garrido-Rodríguez<sup>5,6,7</sup>, Isabel Lastres-Becker<sup>2,8,9,10,11</sup>, Julia Chocarro<sup>2,12</sup>, José L. Lanciego<sup>2,12</sup>, Eduardo Muñoz<sup>5,6,7\*</sup>  and Javier Fernández-Ruiz<sup>1,2,3\*</sup> 

## Abstract

**Background** The cannabigerol derivative VCE-003.2, which has activity at the peroxisome proliferator-activated receptor- $\gamma$  has afforded neuroprotection in experimental models of Parkinson's disease (PD) based on mitochondrial dysfunction (6-hydroxydopamine-lesioned mice) and neuroinflammation (LPS-lesioned mice). Now, we aim to explore VCE-003.2 neuroprotective properties in a PD model that also involves protein dysregulation, other key event in PD pathogenesis.

**Methods** To this end, an adeno-associated viral vector serotype 9 coding for a mutated form of the  $\alpha$ -synuclein gene (AAV9-SynA53T) was unilaterally delivered in the substantia nigra pars compacta (SNpc) of mice. This model leads to motor impairment and progressive loss of tyrosine hydroxylase-labelled neurons in the SNpc.

**Results** Oral administration of VCE-003.2 at 20 mg/kg for 14 days improved the performance of mice injected with AAV9-SynA53T in various motor tests, correlating with the preservation of tyrosine hydroxylase-labelled neurons in the SNpc. VCE-003.2 also reduced reactive microgliosis and astrogliosis in the SNpc. Furthermore, we conducted a transcriptomic analysis in the striatum of mice injected with AAV9-SynA53T and treated with either VCE-003.2 or vehicle, as well as control animals. This analysis aimed to identify gene families specifically altered by the pathology and/or VCE-003.2 treatment. Our data revealed pathology-induced changes in genes related to mitochondrial function, lysosomal cell pathways, immune responses, and lipid metabolism. In contrast, VCE-003.2 treatment predominantly affected the immune response through interferon signaling.

**Conclusion** Our study broadens the neuroprotective potential of VCE-003.2, previously described against mitochondrial dysfunction, oxidative stress, glial reactivity and neuroinflammation in PD. We now demonstrate its efficacy against another key pathogenic event in PD as  $\alpha$ -synuclein dysregulation. Furthermore, our investigation

\*Correspondence:

Eduardo Muñoz

fi1muble@uco.es

Javier Fernández-Ruiz

jjfr@med.ucm.es

Full list of author information is available at the end of the article



© The Author(s) 2024. **Open Access** This article is licensed under a Creative Commons Attribution-NonCommercial-NoDerivatives 4.0 International License, which permits any non-commercial use, sharing, distribution and reproduction in any medium or format, as long as you give appropriate credit to the original author(s) and the source, provide a link to the Creative Commons licence, and indicate if you modified the licensed material. You do not have permission under this licence to share adapted material derived from this article or parts of it. The images or other third party material in this article are included in the article's Creative Commons licence, unless indicated otherwise in a credit line to the material. If material is not included in the article's Creative Commons licence and your intended use is not permitted by statutory regulation or exceeds the permitted use, you will need to obtain permission directly from the copyright holder. To view a copy of this licence, visit <http://creativecommons.org/licenses/by-nc-nd/4.0/>.

sheds light on the molecular mechanisms underlying VCE-003.2 revealing its role in regulating interferon signaling. These findings, together with a favorable ADMET profile, enhance the preclinical interest of VCE-003.2 towards its future clinical development in PD.

**Keywords** VCE-003.2, Parkinson's disease, alpha-synuclein, Cannabinoids, PPAR- $\gamma$

## Introduction

Cannabinoids have emerged as promising neuroprotective agents given their ability to work as pleiotropic compounds against the multiple events that affect neural cell homeostasis, integrity and survival in conditions of brain damage and neurodegeneration [31]. This pleiotropism is facilitated by the activity of cannabinoids at multiple pharmacological targets within the endocannabinoid system (e.g., cannabinoid type-1 (CB<sub>1</sub>), cannabinoid type-2 (CB<sub>2</sub>) and GPR55 receptors, fatty acid amide hydrolase (FAAH) and monoacylglycerol lipase (MAGL) enzymes; see [31], [6, 20, 27, 32]. Additionally, cannabinoids interact with other signaling systems, such as transient receptor potential vanilloid type-1 (TRPV1), peroxisome proliferator-activated receptors (PPARs), adenosine and serotonin receptors [31, 70, 73]. This neuroprotective potential has been preclinically investigated in different neurological conditions, such as accidental brain damage (e.g., stroke, brain trauma, spinal cord injury) and in chronic progressive disorders (e.g., Alzheimer's disease and related dementias, amyotrophic lateral sclerosis, Huntington's disease and others; see [4, 23, 30, 55, 65].

One of the disorders that has recruited more research with cannabinoids to date is Parkinson's disease (PD). Several cannabinoids have been found to be able to alleviate specific parkinsonian symptoms such as bradykinesia and immobility [46], tremor [67] and/or L-DOPA-induced dyskinesia [26]. However, a significantly greater interest has been recruited with those cannabinoid treatments active at preserving neuronal integrity then resulting in delayed disease progression [3, 7, 27, 29, 43]. Such neuroprotective properties include cannabinoid receptor-independent antioxidant effects, mainly afforded by the non-psychoactive phytocannabinoid cannabidiol (CBD), whose structure allows this compound to act as scavenger of reactive oxygen species [51], as well as it modulates the antioxidant transcription factor Nuclear Factor (Erythroid-derived 2)-related factor 2 (NRF-2) pathway too [40]. Activating the CB<sub>1</sub> receptor was furtherly proposed as a neuroprotective therapy in experimental PD in a few studies [22, 62], despite it may aggravate akinetic signs in certain circumstances and produce psychoactive effects (reviewed in Fernández-Ruiz [28], . This has limited the studies with this cannabinoid receptor type and redirected the research to non-psychoactive cannabinoid receptors, for example the CB<sub>2</sub> receptor, whose activation with HU-308,  $\Delta^9$ -tetrahydrocannabivarin ( $\Delta^9$ -THCV), VCE-004.8 and

other agonists entails anti-inflammatory and neuroprotective effects in different experimental models of PD [13, 35, 39, 44, 74]. A similar reduction of inflammatory events, resulting in preservation of nigrostriatal dopaminergic neurons in the basal ganglia, has been found with cannabinoids that are able to target the orphan receptor GPR55, which has been recently associated with the endocannabinoid system [14, 19]. In addition, the activation of PPAR- $\gamma$  with glitazones [78], but also with some cannabinoids (e.g., VCE-003.2, CBGA-Q, GBGA-Q Salt), have been also associated with neuroprotective effects in different experimental models of PD [12, 15, 36]. Collectively, these studies have situated several cannabinoid compounds in a promising position for serving to generate a cannabinoid-based therapy for specific symptoms and, in particular, for disease progression in patients affected by PD (reviewed recently in Jain et al., [43].

Recent studies have demonstrated that an interesting and clinically promising cannabinoid compound in PD is the non-thiophilic and antioxidant CBG quinone derivative VCE-003.2, which behaves as a PPAR- $\gamma$  partial agonist with no activity at the CB<sub>1</sub>/CB<sub>2</sub> receptors [24]. The compound crosses the blood-brain barrier (BBB) after systemic administration [1, 24] and has been investigated here in relation with other preclinical attributes such as metabolism and toxicology. VCE-003.2 shows a favorable profile and rodent pharmacokinetic data guaranteeing high plasma exposure and rapid excretion after its oral administration, which overall may facilitate further translational studies towards the clinical scenario. In our hands, VCE-003.2 has been found to be active as a neuroprotective agent against inflammation-driven neuronal deterioration in LPS-lesioned mice [12, 36], as well as against mitochondrial impairment and oxidative stress in 6-hydroxydopamine (6-OHDA)-lesioned mice [15]. These cytoprotective effects were confirmed in experiments with cell-based models reproducing in vitro the in vivo models, which also revealed that these benefits were mediated by its binding at a functional alternative site (different from the canonical binding site used by glitazones) in the PPAR- $\gamma$  receptor [15, 36]. We are now interested in further reinforcing the neuroprotective profile of VCE-003.2 in PD using experimental models based on protein ( $\alpha$ -synuclein) dysregulation and accumulation, a key event in PD pathogenesis.  $\alpha$ -Synuclein is a key protein in the formation of Lewy bodies in which this protein is a major component [69]. Their mutations have been associated with autosomal dominant or

recessive forms of genetic PD, whereas gene duplications or triplications have been also associated with the genetic parkinsonism (reviewed in Marmion and Kordower [56]). To this end, we used a murine model based on the local overexpression of  $\alpha$ -synuclein carrying the A53T mutation, which is one of the most frequent mutation used in experimental models of PD, in the substantia nigra pars compacta (SNpc) through the local application of an adeno-associated viral vector serotype 9 (AAV9) encoding the mutated gene, as previously used in other preclinical studies [18, 45, 48, 66]; see details in a recent review by Björklund and Mattsson [10]. The local overexpression of A53T  $\alpha$ -synuclein in the SN leads to a pathological phenotype visible in a short time (2 weeks after viral inoculation) consisting in motor defects,  $\alpha$ -synuclein dysregulation, loss of dopaminergic neurons, autophagy induction, and microglial reactivity [18, 66]. Using these mice, we have investigated the neuroprotective potential of a chronic oral administration of VCE-003.2 by analyzing whether this cannabigerol derivative prevents behavioural, biochemical, and histopathological alterations elicited by A53T  $\alpha$ -synuclein accumulation. The analysis of nigral dopaminergic neurons was carried out using first classic immunostaining, but the results were furtherly confirmed with a stereological-like procedure based on a deep-learning dedicated algorithm (Aiforia<sup>®</sup>) that has been successfully validated and published by Penttinen et al. [61]. It presently represents a useful tool with significant advantages (mainly reproducibility, elimination of human error, and fast high-capacity analysis) compared to unbiased stereological analysis. In our hands, it has been used with success in previous studies [21, 63]. Transcriptomic analysis of the striatum identified possible genes and pathways underlying the beneficial effects of VCE-003.2, as well as some of them related to the pathology.

## Materials and methods

### Viral vector production

A recombinant AAV vector serotype 2/9 expressing the *SNCA* gene with A53T mutation driven by the human synapsin promoter was produced by Vector Builder ([www.vectorbuilder.com](http://www.vectorbuilder.com); catalog No. P211024-1010fpa; lot No. 211221AAVJ03). The virus was formulated in PBS buffer (pH 7.4) supplemented with 200 nM NaCl and 0.001% pluronic F-68. Obtained vector concentration was  $9.62 \times 10^{13}$  GC/ml. Virus purity was determined by SDS-PAGE followed by silver staining, resulting in >80% pure. Plasmid map for pAAV-synapsin-SynA53T and sequence are provided in Supplementary File 1.

### Animals and surgical lesions

Male C57BL/6 mice were housed in our animal facilities (CAI-Animalario, Faculty of Medicine, Complutense

University, ref. ES280790000086) in a room with a controlled photoperiod (08:00–20:00 light) and temperature ( $22 \pm 1^\circ\text{C}$ ). They had free access to standard food and water and were used at adult age (6–8-month-old; weight=28–33 g). All animal experiments were conducted by researchers having the necessary accreditation and following local, national and European guidelines (directive 2010/63/EU), as well as conformed to ARRIVE guidelines and were approved by our local Ethical Committee for Animal Experimentation (ref: PROEX 201.8/22).

Mice were used for the *in vivo* overexpression of human  $\alpha$ -synuclein with the A53T mutation using recombinant AAV9 encoding for this gene under the control of human synapsin 1 promoter. To this purpose, mice were anaesthetized (ketamine 40 mg/kg+xylazine 4 mg/kg, *i.p.*) and subjected to unilateral injections of viral particles (AAV9-SynA53T) into the SNpc of the right hemisphere following the procedure described in Lastres-Becker et al. [52]. In brief, 1  $\mu\text{l}$  of a viral suspension containing  $3.33 \times 10^{12}$  GC/ml (selected from a preliminary concentration-response experiment using a range for the viral suspension of  $3.33 \times 10^{12}$  –  $3.33 \times 10^{13}$  GC/ml) was unilaterally injected at predefined stereotaxic coordinates: -2.5 mm posterior to bregma, -1.4 mm lateral to midline and -4.5 mm ventral to dura. The volume of 1  $\mu\text{l}$  was pressure-injected in pulses of 0.2  $\mu\text{l}/\text{min}$  and, once completed, the needle was left in place for 5 min before withdrawal to minimize reflux of viral suspension through the injection tract. Control animals were sham-operated and injected with 1  $\mu\text{l}$  of a viral suspension of an empty AAV9 (AAV9-null) containing  $1.07 \times 10^{12}$  GC/ml using the same coordinates. The lesions were generated using unilateral inoculation, so that contralateral structures serve as controls for the different analyses (see Fig. 1 for a diagram showing the schedule used).

### Pharmacological treatments and sampling

After the application of AAV9-SynA53T or control AAV9-null vectors, animals were distributed into 3 groups in each experiment, and were subjected to a daily treatment with VCE-003.2 (20 mg/kg), or vehicle (sesame oil) by oral administration (see Fig. 1 for a diagram showing the schedule used). The number of animals in each experimental group was: (i) vehicle-treated sham-operated mice: 4–6; (ii) vehicle-treated AAV9-SynA53T mice: 8–10; and (iii) VCE-003.2-treated AAV9-SynA53T mice: 8–10 (ranges are due to elimination of potential outliers in those cases that the statistical analysis recommended to do it). The first administration, in all cases, was done approximately 24 h after the lesion and the treatment was prolonged for two weeks. At the end of the treatment (24 h after the last injection), they were analysed in different behavioural tests just before being killed by

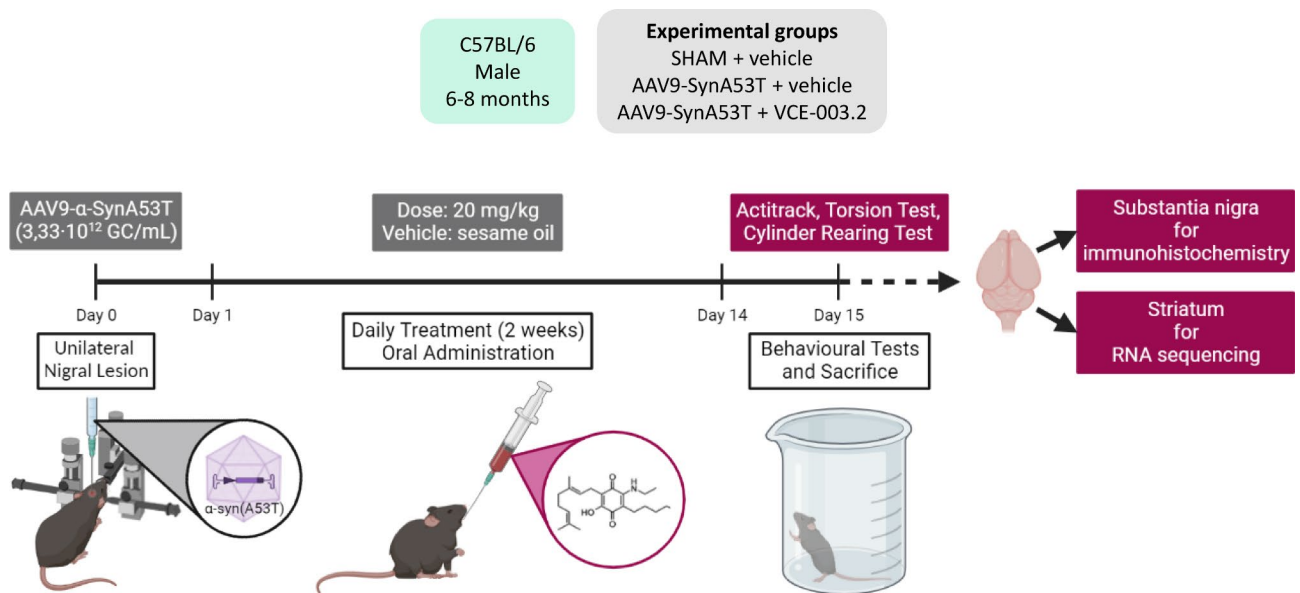


**Fig. 1** Representative scheme of the experimental protocol used for the induction of  $\alpha$ -synuclein-based PD model used in this study and the treatment with VCE-003.2, with indication of timelines for treatments, behavioral analysis and animal euthanasia

rapid and careful decapitation, and their brains rapidly removed and divided coronally in two parts. The anterior halves were used to dissect the striatum. Tissues were rapidly frozen by immersion in cold 2-methylbutane and stored at  $-80^{\circ}\text{C}$  for RNA sequencing analysis (RNAseq). The posterior halves containing the midbrains were fixed for one day at  $4^{\circ}\text{C}$  in fresh 4% paraformaldehyde prepared in 0.1 M PBS, pH 7.4. Samples were cryoprotected by immersion in a 30% sucrose solution for a further day, and finally stored at  $-80^{\circ}\text{C}$  for immunohistochemical analysis in the SN.

#### Pharmacokinetic and ADMET analysis

Pharmacokinetic for oral VCE-003.2 in mice and in vitro off-target binding, transporter interactions, micronucleus assay, and comparative metabolism assays for VCE-003.2 in hepatocytes from different species were performed by Charles River (Edinburgh, UK) and Eurofins Panlabs Discovery Services (New Taipei City, TW), using protocols summarized in Supplementary File 2.

#### Behavioural tests

**Cylinder rearing test (CRT)** Given that the lesions were unilateral, this test attempts to quantify the degree of forepaw (ipsilateral, contralateral, or both) preference for wall contacts in rearing movements after placing the mouse in a methacrylate transparent cylinder (diameter: 15.5 cm; height: 12.7 cm; Fleming et al., [33]). Each score was calculated from a 3 min trial with a minimum of 4 wall contacts. See Supplementary File 3 for an example of video recording in the three experimental groups.

**Elevated-body swing test (EBST)** Mice were placed head-downward hanging by their tail in a vertical axis (about 15 cm from the surface) and recorded for 60 s [8, 11]. A swing was recorded whenever the animal moved its head out of the vertical axis to either side, whereas for the next swing to be counted, the animal must have returned to the vertical position first. See Supplementary File 4 for an example of video recording in the three experimental groups.

**Computer-aided Actimeter** For the analysis of motor activity, we used a computer-aided actimeter (Actitrack, Panlab, Barcelona, Spain). This apparatus consisted of a  $45 \times 45$  cm area, with infra-red beams all around, spaced 2.5 cm, coupled to a computerized control unit that analyzes the following parameters: (i) distance run in the actimeter (ambulation); (ii) time spent in inactivity; (iii) frequency of vertical activity (rearing); (iv) mean and maximal velocity developed during the running; and (v) time spent in fast ( $>5$  cm/s) and slow ( $<5$  cm/s) movements. Animals remained for a period of 10 min in the actimeter, but measurements were only recorded during the final 5 min (first 5 min was used only for animal acclimation). These data are presented as Supplementary File 5.

#### Immunohistochemical procedures

Brains were sliced in coronal sections (containing the SN) in a cryostat ( $30\ \mu\text{m}$  thick) and collected in anti-freeze solution (glycerol/ethylene glycol/PBS, 2:3:5) and stored at  $-20^{\circ}\text{C}$  until being used. Brain sections were mounted on gelatine-coated slides, and once adhered, washed in 0.1 M potassium PBS (KPBS) at pH 7.4. Then,

endogenous peroxidase was blocked by 30 min incubation at room temperature in peroxidase blocking solution (Dako Cytomation, Glostrup, Denmark). After several washes with KPBS, sections were incubated overnight at 4°C with the following antibodies: (i) monoclonal mouse anti-human  $\alpha$ -synuclein (sc-53955; Santa Cruz Biotechnology, Dallas, TX, USA) used at 1:2000; (ii) polyclonal rabbit anti-mouse tyrosine hydroxylase (TH) (AB152; Chemicon-Millipore, Temecula, CA, USA) used at 1:200; (iii) polyclonal rat anti-mouse CD68 antibody (MCA-1957; AbD Serotec, Oxford, UK) used at 1:200; or (iv) polyclonal rabbit anti-mouse GFAP antibody (Z0334; Dako Cytomation, Glostrup, Denmark) used at 1:200. Dilutions were carried out in KPBS containing 2% bovine serum albumin and 0.1% Triton X-100 (Sigma Chem., Madrid, Spain). After incubation, sections were washed in KPBS, followed by 1 hour incubation at room temperature with the corresponding biotinylated secondary antibody (1:1000 for  $\alpha$ -synuclein; 1:200 for the rest) (Vector Laboratories, Burlingame, CA, USA) for 1 hour at room temperature. Avidin-biotin complex (Vector Laboratories, Burlingame, CA, USA) and 3,3'-diaminobenzidine substrate-chromogen system (Dako Cytomation, Glostrup, Denmark) were used to obtain a visible reaction product. Negative control sections were obtained using the same protocol with omission of the primary antibody. A Leica DMRB microscope and a DFC300FX camera (Leica, Wetzlar, Germany) were used for the observation and photography of the slides, respectively. For quantification of the intensity of  $\alpha$ -synuclein, TH, CD68 or GFAP immunostaining in the SN (at both ipsilateral and contralateral sides), we used the NIH Image Processing and Analysis software (ImageJ; NIH, Bethesda, MD, USA) using 4–5 sections, separated approximately by 200  $\mu$ m, and observed with 5x–20x objectives depending on the immunostaining under quantification. In all sections, the same area of the SNpc was analysed. Analyses were always conducted by experimenters who were blinded to all animal characteristics. Data were expressed as percentage of immunostaining intensity in the ipsilateral (lesioned) side over the contralateral (non-lesioned) side. In addition, in the case of CD68 immunostaining, images at higher magnification were also used for a qualitative analysis of certain morphological characteristics (cell body volume; number, thickness and length of cell processes) that may reflect the state of quiescence (low cell body volume and tiny and long processes) or activation (amoeboid-like morphology: high cell body volume and thick and short processes) of these cells.

In a further analysis, a deep-learning dedicated algorithm was prepared with Aiforia® [61], validated and released (resulting in an error of 4.82%) for quantifying the number of TH-positive neurons in TH-stained, equally-spaced coronal sections covering the whole

rostrorocaudal extent of the SNpc. The dedicated algorithm was customized to count all positive neurons, independently of the intensity of staining. Sections were scanned at 20x in a slide scanner (Aperio CS2; Leica, Wetzlar, Germany) and uploaded to the Aiforia® cloud. Next, the boundaries of each selected ROI were outlined at low magnification and the dedicated algorithm was then used as a template quantifying the TH-positive neurons. Details on this analysis have been previously published [21, 63].

### Transcriptomic analysis

**RNA isolation and sequencing** RNA was isolated from the striatum samples using the RNeasy Lipid Tissue Mini kit (Qiagen, Barcelona, Spain) following the manufacturer's instructions, including the optional DNase I step. Once RNA was isolated, samples were stored at  $-80^{\circ}\text{C}$  following library preparation. RNA concentration and RNA integrity number (RIN) was assessed using Nanodrop and Bioanalyzer (Centre for Genomic Regulation, Barcelona, Spain). Library preparation and sequencing was outsourced to the Centre for Genomic Regulation (CRG, Barcelona, Spain). Briefly, libraries were prepared using the TruSeq mRNA Library prep following the manufacturer's instructions. mRNA selection was performed using poly(A)-mRNA selection strategies. Libraries were prepared and sequenced by 50 bp sequencing using Illumina NextSeq 2000 run system (Illumina, Inc., San Diego, CA, USA).

**RNA-seq data processing and normalization** Raw reads were aligned against the GRCm38 genome (v84) from ENSEMBL with HISAT2 (v2.1.0) [47, 59]. This resulted in a  $\sim 99\%$  alignment rate with 60% of reads aligned to exonic regions. The count matrix was obtained from the alignments using the corresponding ENSEMBL annotation file with featureCounts (v2.0.0) [54]. Then, counts per million (CPM) were calculated using CPM function from the EdgeR packing in R [53]. Lowly expressed genes were filtered out, which were defined as having less than one CPM in at least 25% of the samples leading to a total of 13,980 genes. Principal Component Analysis (PCA) was used to identify sources of variation and outliers. As samples were sequenced in two independent batches, we regressed out sequencing batch to control variation. The final dataset was composed by 17 samples (6 from vehicle-treated sham-operated mice, 5 vehicle-treated AAV9-SynA53T-injected mice, and 6 VCE-003.2-treated AAV9-SynA53T-injected mice).

**Differential expression analysis** Differential expression analysis was performed using the R package limma [64]. EdgeR was used for data normalization using TMM values and followed by voom transformation. *P*-values were corrected using the Benjamini-Hochberg false discovery rate (FDR).

**Pathway enrichment analysis.** We used Gene Set Enrichment Analysis (GSEA) focusing on Hallmark gene sets [72]. To perform pathway analysis, ranked DEGs in terms of t-value were used as input. We used the fGSEA R-package [49]. Only pathways with adjusted  $P$ -value < 0.05 were considered.

**Transcription factor enrichment analysis** For exploring if genes were enriched for specific transcription factors, we used DoRothEA [37, 41]. Regulons were filtered at confidence levels “A” and “B”. Regulon enrichment was runned using fgsea with preranked data in terms of t value. Only regulons with adjusted  $P$ -value < 0.05 were considered.

### Statistics

Data were assessed using one-way ANOVA, followed by the Tukey test using GraphPad Prism, version 8.00 for Windows (GraphPad Software, San Diego, CA, USA). A  $p$  value lower than 0.05 was used as the limit for statistical significance. The sample sizes in the different experimental groups were always  $\geq 5$ .

## Results

### Pharmacokinetic, metabolic, and toxicological properties of VCE-003.2

We have previously shown that VCE-003.2 crossed the BBB after oral administration in rats [1]. Now, we extended our PK studies in mice, found that plasma VCE-003.2 levels peaked at 4 h ( $T_{max}$ ) and then slowly declined to basal levels at 24 h. Oral VCE-003.2 resulted in 69% bioavailability ( $F$ ) in mice (Supplementary Table 1), which was significantly higher than the one observed in rats ( $F=13,77\%$ ) [1]. Moreover, VCE-003.2 did not significantly inhibit the activity of relevant cytochrome P450 isoforms, did not inhibit hERG channel activity and it was not genotoxic as assessed by AMES assays [1]. To complement these studies, we interrogated for potential off-targets and genotoxicity of VCE-003.2. Using radioligand binding assays, we explored the interaction with a panel of 172 receptors and channels, and we found that VCE-003.2 did not show a significant binding activity to these targets (Supplementary File 2). The potential genotoxicity of VCE-003.2 was investigated using micronucleus assays either in the presence or absence of a metabolic activation system (S9-mix), in cultured human lymphocytes (in vitro) and in rat bone marrow cells (in vivo). We observed that VCE-003.2 is not clastogenic or aneugenic either in human lymphocytes or in the bone marrow micronucleus test of male rats up to a dose of 2000 mg/kg (Supplementary File 2).

We also investigated the metabolic stability and metabolite profiles of VCE-003.2 using suspensions of cryopreserved hepatocytes from CD-1 mouse, Wistar rat, Beagle dog, Göttingen minipig, cynomolgus monkey and

human. The rates of metabolism and the metabolite profiles were compared across the species tested. Twenty-six metabolites of VCE-003.2 were found in the hepatocyte incubations of the six species investigated. Based on the MS peak intensities, no human specific metabolites were observed and five major metabolites of VCE-003.2 were detected in at least four of the six species tested. Metabolic reactions observed included oxidations, the loss of  $C_3H_6$  in combination with two oxidations, and a desaturation in combination with one or two oxidations. The postulated major metabolic pathway VCE-003.2 was also predicted (Supplementary File 2).

Finally, we explored the in vitro interaction of VCE-003.2 with human BCRP, BSEP and MDR1 efflux (ABC) transporters, and with human solute carrier (SLC) transporters MATE1, MATE2-K, OAT1, OAT3, OATP1B1, OATP1B3, OCT1 and OCT2. VCE-003.2 did not inhibit SLC transported and up to 22.5  $\mu$ M showed inhibitory activity of the ABC transporters (BCR=89% inhibition, BSEP=less than 50% inhibition; MDR1=81% inhibition) (Supplementary File 2). Altogether, VCE-003.2 represents an excellent ligand for studying the relevance of PPAR- $\gamma$  activation in experimental models of PD, as has been demonstrated in previous studies [12, 15, 36] and situates this compound in a clear advantage for future translational development.

### Behavioural readouts of treatment with VCE-003.2 in mice injected with AAV9-SynA53T

To explore the neuroprotective potential of an oral administration of VCE-003.2 against the overexpression of neuronal (A53T) $\alpha$ -synuclein, we first analysed the motor performance of these animals using CRT and EBTS. These motor tests discriminate the unilateral hemiparesis and were assessed 24 h after the last VCE-003.2 administration, avoiding any acute effect of the drug. CRT showed a preference for the ipsilateral right paw (controlled by the non-lesioned contralateral SN) in mice-injected with AAV9-SynA53T, which was prevented by the treatment with VCE-003.2 ( $F(2,17)=11.50$ ,  $p<0.001$ ; Fig. 2 and Supplementary File 3). Also, we noticed a general mobility increase, reflected in the total number of rearings, in the VCE-003.2-treated animals, which tended to be elevated with respect to both vehicle-treated sham-operated and AAV9-SynA53T-injected mice ( $F(2,18)=2.99$ ,  $p=0.075$ ; Fig. 2).

Next, we performed EBST, which is useful to detect the side more frequent in the torsion movements depending on the lesioned side. We found that vehicle-treated AAV9-SynA53T-injected mice tended to show a preference for contralateral turns, which was not attenuated by the treatment with VCE-003.2, even it tended to be enhanced ( $F(2,19)=1.49$ , ns; Fig. 2 and Supplementary File 4). However, as in CRT, we observed a higher number

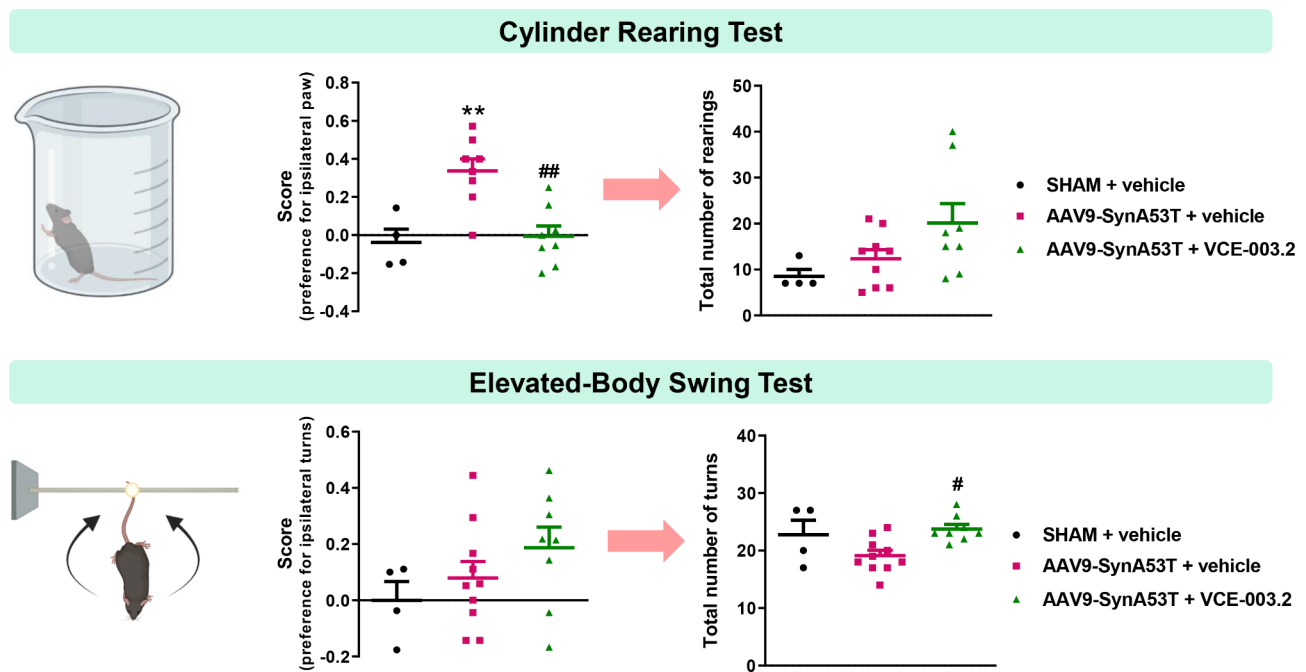


**Fig. 2** Behavioural analysis in the Cylinder Rearing Test (CRT) and in the Elevated-Body Swing Test (EBST) of vehicle-treated control (sham-operated) adult male mice and unilaterally AAV9-SynA53T-injected adult male mice treated with vehicle or VCE-003.2 (20 mg/kg) given orally. Treatments were daily and prolonged for 2 weeks. Data (preference score (left) and total number of movements (right)) corresponded to 24 h after the last dose and were expressed as means  $\pm$  SEM of more than 4 animals per group. They were analyzed by one-way ANOVA followed by the Tukey test (\*\* $p < 0.01$  versus vehicle-treated sham-operated mice; # $p < 0.05$ , ## $p < 0.01$  versus vehicle-treated AAV9-SynA53T-injected mice)

of total turns (irrespective of the side) shown during the test performance ( $F(2,19)=5.13$ ,  $p < 0.05$ ; Fig. 2), demonstrating a greater activity in the treated animals.

Such elevated motor activity elicited by VCE-003.2 in AAV9-SynA53T-injected mice in comparison with the other two groups was also visible in the data obtained in a computer-aided actimeter (actitrack), with statistically significant increases in locomotor parameters such as general activity ( $F(2,19)=4.39$ ,  $p < 0.05$ ), ambulation ( $F(2,19)=4.55$ ,  $p < 0.05$ ), mean and maximal velocities ( $F(2,19)=4.14$ ,  $p < 0.05$  and  $F(2,19)=5.53$ ,  $p < 0.05$ , respectively), and frequency of slow movements ( $F(2,19)=5.82$ ,  $p < 0.01$ ). This increase remained as a mere numerical trend in parameters as vertical activity ( $F(2,19)=1.56$ ,  $p=0.24$ ) and frequency of fast movements ( $F(2,19)=2.65$ ,  $p=0.096$ ), whereas the opposite (lower values) was detected, as expected, for resting time ( $F(2,19)=5.13$ ,  $p < 0.05$ ), then confirming that VCE-003.2-treated AAV9-SynA53T-injected mice frequently exhibited a greater motor activity (see these data in the Supplementary File 5).

#### Histopathological readouts of treatment with VCE-003.2 in mice injected with AAV9-SynA53T

Immunohistochemical analysis demonstrated an AAV9-driven overexpression of human  $\alpha$ -synuclein all over the midbrain in the lesioned mice, in particular in the SNpc

( $F(2,18)=19.42$ ,  $p < 0.0001$ ; see Supplementary File 6) [18, 66]. Furthermore, the enhanced neuronal expression of mutated  $\alpha$ -synuclein was associated with a significant reduction (around 35%) of TH immunoreactivity in the SNpc ( $F(2,21)=20.67$ ,  $p < 0.0001$ ; Fig. 3). Treatment with VCE-003.2 of mice injected with AAV9-SynA53T did not alter the immunoreactivity levels of  $\alpha$ -synuclein (Supplementary File 6). However, it prevented the reduction in TH immunoreactivity to the same value detected in sham-operated mice (Fig. 3). This observation supports the idea that VCE-003.2 treatment preserves the integrity of TH-positive neurons in the SNpc against the enhanced neuronal expression of mutated  $\alpha$ -synuclein, despite our analysis only served to measure immunoreactivity levels. In a further analysis, using a stereological-like analysis based on a deep-learning dedicated algorithm (Aiforia<sup>®</sup>), we could confirm that the reduction in TH measured in the SNpc of mice injected with AAV9-SynA53T, as well as the recovery detected after the treatment with VCE-003.2, reflected both a loss and a preservation in the number of TH-positive neurons, respectively ( $F(2,21)=6.72$ ,  $p < 0.01$ ; see Supplementary File 7). This preservation may contribute to the behavioral improvements indicated in the previous subsection.

The neuronal overexpression of mutated  $\alpha$ -synuclein in the SN also induced robust glial reactivity in both microglia (CD68:  $F(2,17)=27.58$ ,  $p < 0.0001$ ; Fig. 4), and

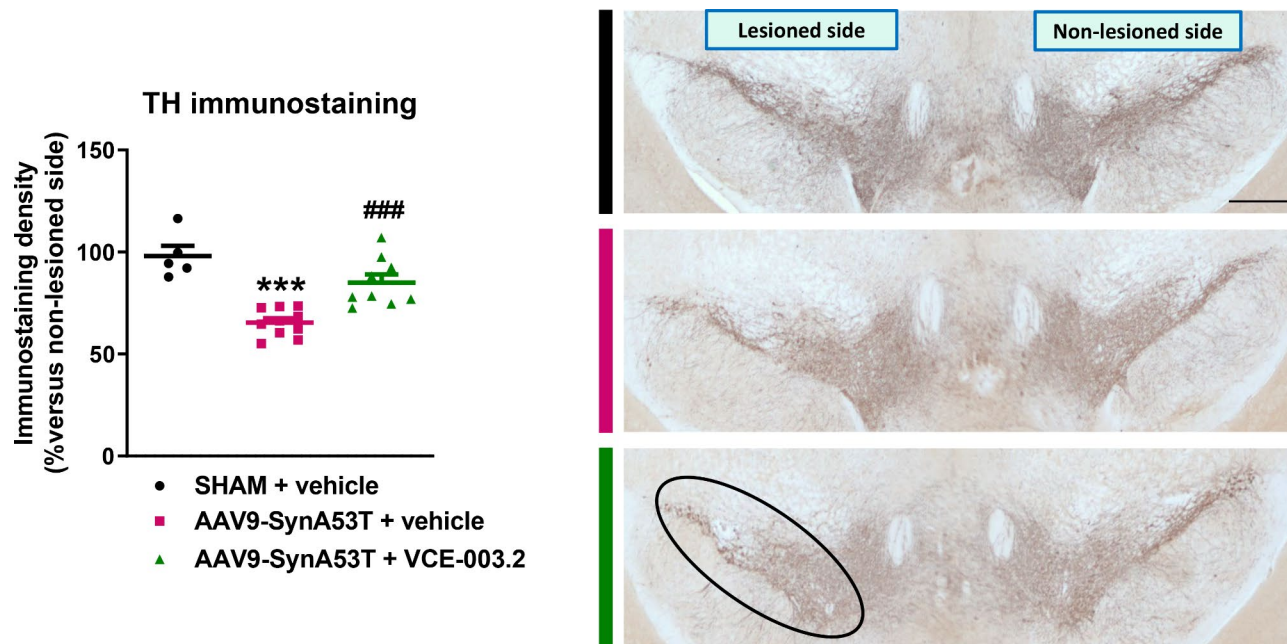


**Fig. 3** Intensity of the immunostaining for TH measured in a selected area of the SNpc of vehicle-treated control (sham-operated) adult male mice and unilaterally AAV9-SynA53T-injected adult male mice treated with vehicle or VCE-003.2 (20 mg/kg) given orally. Treatments were daily and prolonged for 2 weeks. Data corresponded to 24 h after the last dose and were expressed as means  $\pm$  SEM of more than 5 animals *per* group. They were analyzed by one-way ANOVA followed by the Tukey test ( $***p < 0.005$  versus vehicle-treated sham-operated mice;  $###p < 0.005$  versus vehicle-treated AAV9-SynA53T-injected mice). Representative immunostaining images for each experimental group, with indication of the approximate area quantified, are shown in right panels (scale bar = 200  $\mu$ m)

astrocytes (GFAP:  $F(2,21)=26.17$ ,  $p < 0.0001$ ; Fig. 4 and representative images in Supplementary File 8). In addition, a simple morphological analysis of CD68-labelled cells revealed a higher presence of cells with apparently amoeboid aspect (greater cell body volume and thick and short cells branches) in the SN of vehicle-treated AAV9-SynA53T mice compared to vehicle-treated sham-operated mice (Supplementary File 9), which is compatible with an activated state of these cells. VCE-003.2 treatment attenuated both responses, with a statistically significant effect in CD68 immunostaining (Fig. 4) and a numerical trend in GFAP immunostaining (Fig. 4 and representative images in Supplementary File 8). VCE-003.2 treatment of AAV9-SynA53T mice also reduced the number of CD68-labelled cells with apparently activated phenotype to a more quiescent state (smaller cell bodies and more, tiny and longer processes) (Supplementary File 9).

#### Transcriptomic readouts of treatment with VCE-003.2 in mice injected with AAV9-SynA53T

Having established the neuroprotective efficacy of VCE-003.2 in this  $\alpha$ -synuclein model of PD, and recognizing that functional recovery likely involves the survival of nigrostriatal terminals arising the striatum, we aimed sought to delve into downstream cellular pathways through transcriptomic analysis of this specific brain

region. To this end, we carried out RNA-Seq analysis in the right (lesioned) striatum of mice from the three different experimental groups (Supplementary Table 2). We first examined the impact of  $\alpha$ -synuclein lesion on gene expression, comparing the AAV9-SynA53T-injected mice *versus* sham-operated animals, all treated with vehicle. We did observe a strong transcriptomic dysregulation with 1055 differentially expressed genes (DEGs) at  $FDR < 0.05$  (50.8% up-regulated and 49.2% down-regulated) (Fig. 5, left panel; Supplementary Table 3). The oral administration of VCE-003.2 in the AAV9-SynA53T-injected mice produced a much more modest effect, with only 14 genes (*Irf2*, *Ifitm3*, *Ifit1*, *Ifit3*, *Oasl2*, *H2-Q6*, *Mir6236*, *Lgals9*, *Samd9*, *B2m*, *Oas2*, *H2-K1*, *H2-D1* and *ligp1*) becoming significantly altered from their expression in vehicle-treated AAV9-SynA53T-injected mice, most of them up-regulated, with 9 additional genes being close to be statistically significant (Fig. 5, right panel; Supplementary Table 4). Interestingly, these 23 genes appear to be part of a network of proteins related to interferon biology, as confirmed through Local Network Cluster Analysis using STRING (data not shown). The treatment with VCE-003.2 in AAV9-SynA53T-injected mice did not alter the expression of genes encoding for cannabinoid receptors or for those enzymes involved in the endocannabinoid synthesis and degradation in comparison with those animals treated with vehicle, despite

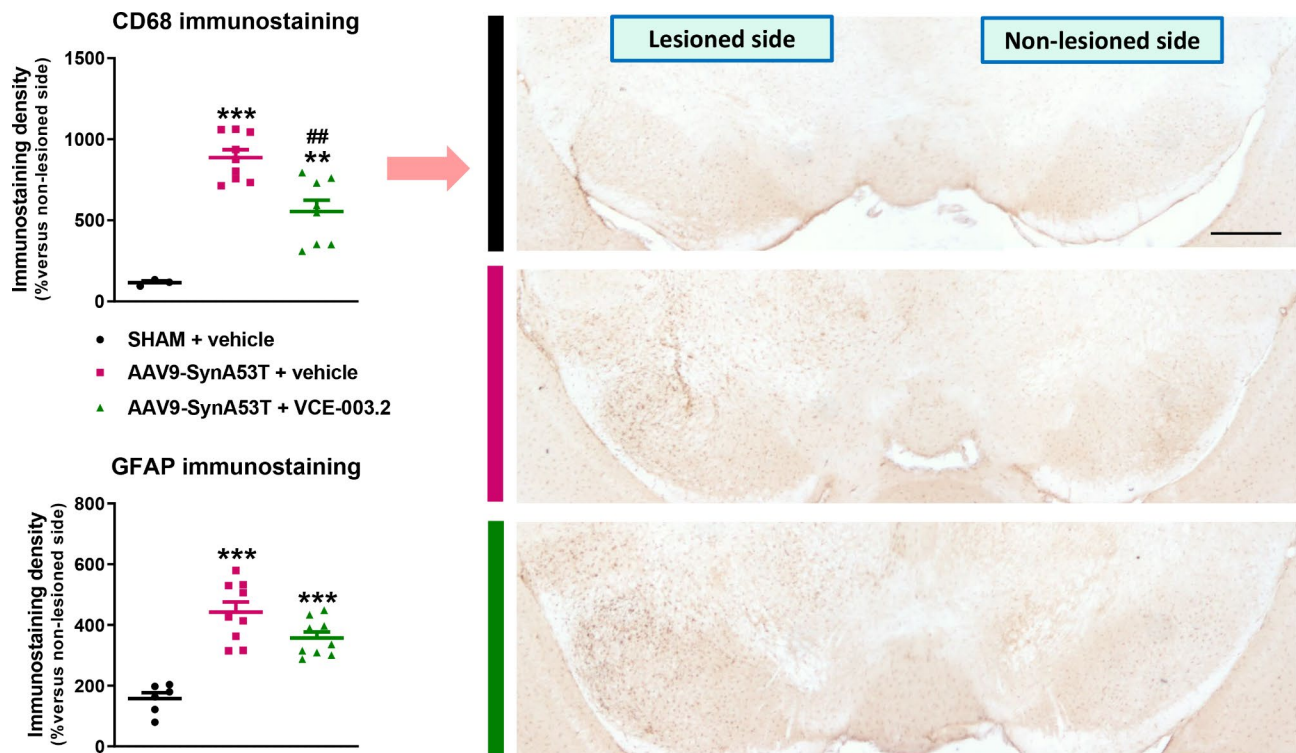


**Fig. 4** Intensity of the immunostaining for CD68 and GFAP measured in a selected area of the SN of vehicle-treated control (sham-operated) adult male mice and unilaterally AAV9-SynA53T-injected adult male mice treated with vehicle or VCE-003.2 (20 mg/kg) given orally. Treatments were daily and prolonged for 2 weeks. Data corresponded to 24 h after the last dose and were expressed as means  $\pm$  SEM of more than 5 animals *per* group. They were analyzed by one-way ANOVA followed by the Tukey test (\*\* $p < 0.01$ , \*\*\* $p < 0.005$  versus vehicle-treated sham-operated mice; ## $p < 0.01$  versus vehicle-treated AAV9-SynA53T-injected mice). Representative CD68 immunostaining images for each experimental group are shown in right panels (scale bar = 200  $\mu$ m)

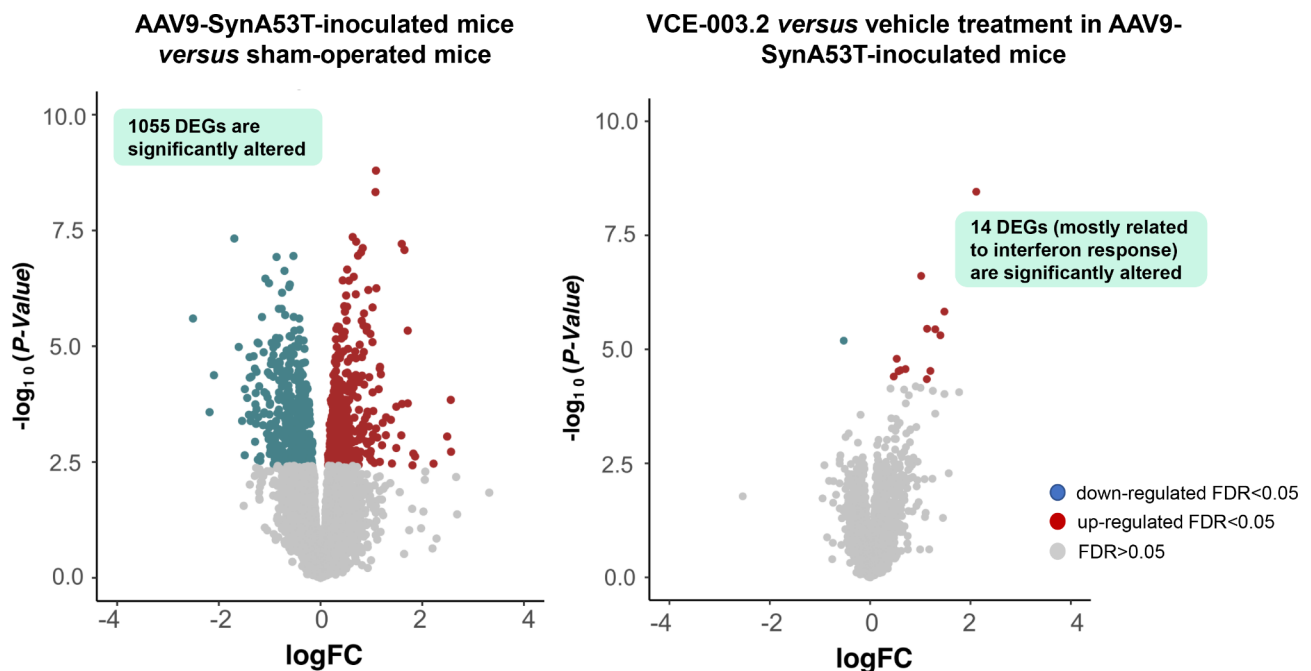


**Fig. 5** Volcano plots showing differentially expressed genes (DEGs). X-axis shows the  $\log_{10}(FC)$  and Y-axis shows  $-\log_{10}(P\text{-value})$ . Every dot represents a specific gene (black are genes at  $FDR > 0.05$  and red are genes at  $FDR < 0.05$ ). Left panel: Volcano plot of the DEGs of AAV9-SynA53T-injected mice versus sham-operated mice, both treated with vehicle. Right panel: Volcano plot of the DEGs of VCE-003.2-treated AAV9-SynA53T-injected mice versus those treated with vehicle. DEGs were observed at  $FDR < 0.05$

some of them did result altered by the local injection of AAV9-SynA53T into the SN. This was the case of the *Cnr1* (down-regulated: logFC=-1.068; FDR=0.007) and the *Gpr55* (up-regulated: logFC=+1.14; FDR=0.006) encoding the CB<sub>1</sub> and GPR55 receptors, respectively, as well as the *Faah* gene (down-regulated: logFC=-0.47; FDR=0.029) encoding the FAAH enzyme (Supplementary Tables 3 and 4). As regards to some PD-related proteins (e.g.,  $\alpha$ -synuclein, parkin, leucine-rich repeat kinase-2 (LRRK2)), our data indicated an important and expected up-regulation of *Snca* gene (logFC=0.48; FDR=0.0058) by the local injection of AAV9-SynA53T into the SN, but not in *Prkn* or *Lrrk2*, and no effect of the VCE-003.2 in any of these three genes (Supplementary Tables 3 and 4).

To understand the biological implications of the transcriptomic dysregulation, we performed GSEA using Hallmark Pathways from Gene Ontology. Pathway analysis revealed that DEGs affected by mutated  $\alpha$ -synuclein overexpression were enriched for pathological hallmarks (see Supplementary Table 5) such as an impaired

mitochondrial function affecting the oxygen species pathway and the oxidative phosphorylation (Fig. 6 and Supplementary Table 5). We also observed down-regulation in pathways associated with autophagy and lysosomal function (e.g., mTORC1 signaling), as well as lipid metabolism (e.g., fatty acid metabolism, adipogenesis) and the interferon response (Fig. 6 and Supplementary Table 5). In contrast, treatment with VCE-003.2 led to a significant increase in the expression of genes related to the interferon signaling, which was the opposite response when compared with the one detected after the delivery of AAV9-SynA53T (Fig. 6 and Supplementary Table 5).

To determine whether the observed transcriptomic dysregulation was orchestrated by specific transcription factors, we conducted regulon enrichment analysis using DoRoThEA [37, 41]. In a first set of analysis, we detected a significant enrichment in several regulons, which were down-regulated in vehicle-treated AAV9-SynA53T-injected mice with respect to vehicle-treated sham-operated animals (Fig. 7; see Supplementary Table 6). Among them was the finger family transcription factor Specificity

## Pathway enrichment (Hallmark pathways)

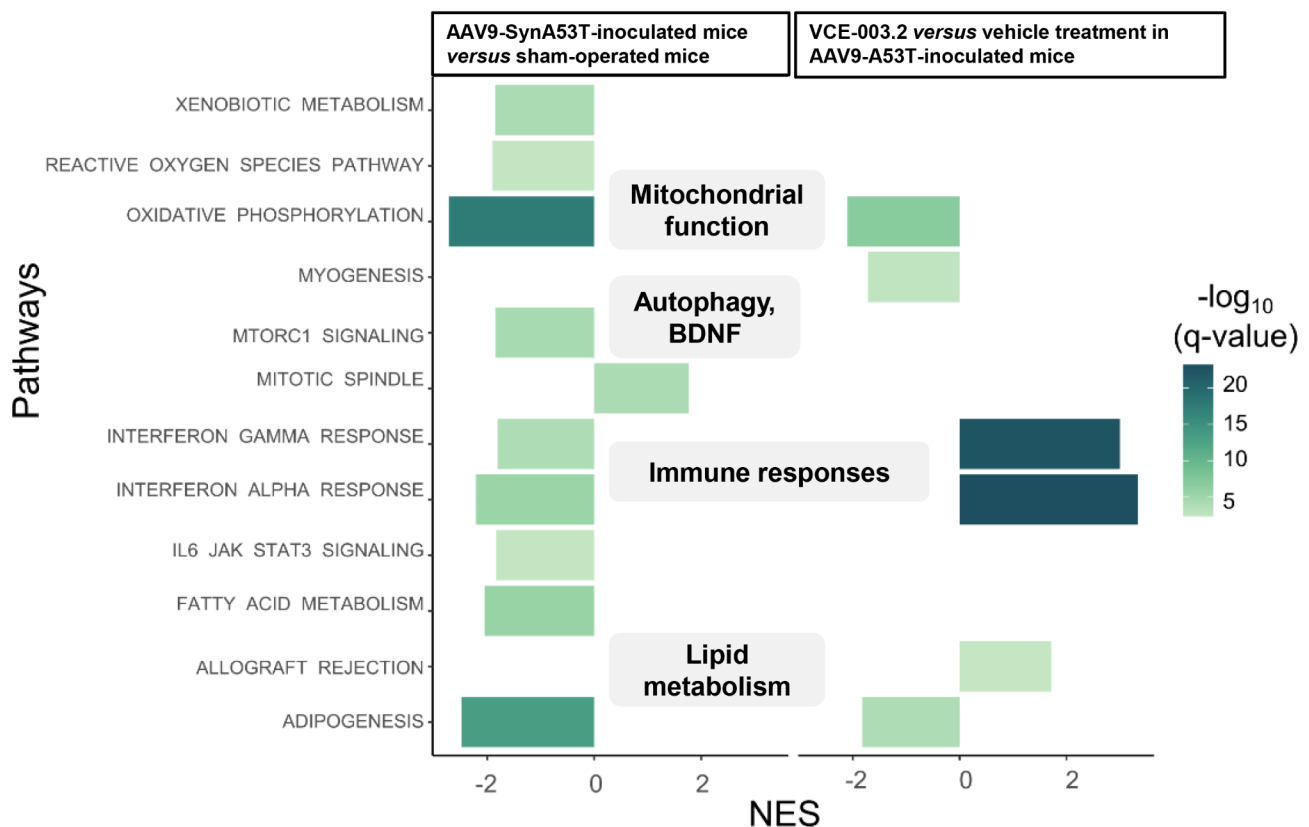


**Fig. 6** Pathway enrichment analysis using Hallmark Pathways from GO using pre-ranked GSEA. Pathways represented are significant at q-value < 0.05. X-axis shows the directionality and Y-axis the biological pathway, with the green color tone reflecting the levels of significance. The significant enrichment for the comparison of AAV9-SynA53T-injected mice versus sham-operated mice, both treated with vehicle, is presented on the left, whereas the one for the comparison of VCE-003.2-treated AAV9-SynA53T-injected mice versus those treated with vehicle is presented on the right

## Transcription factor enrichment

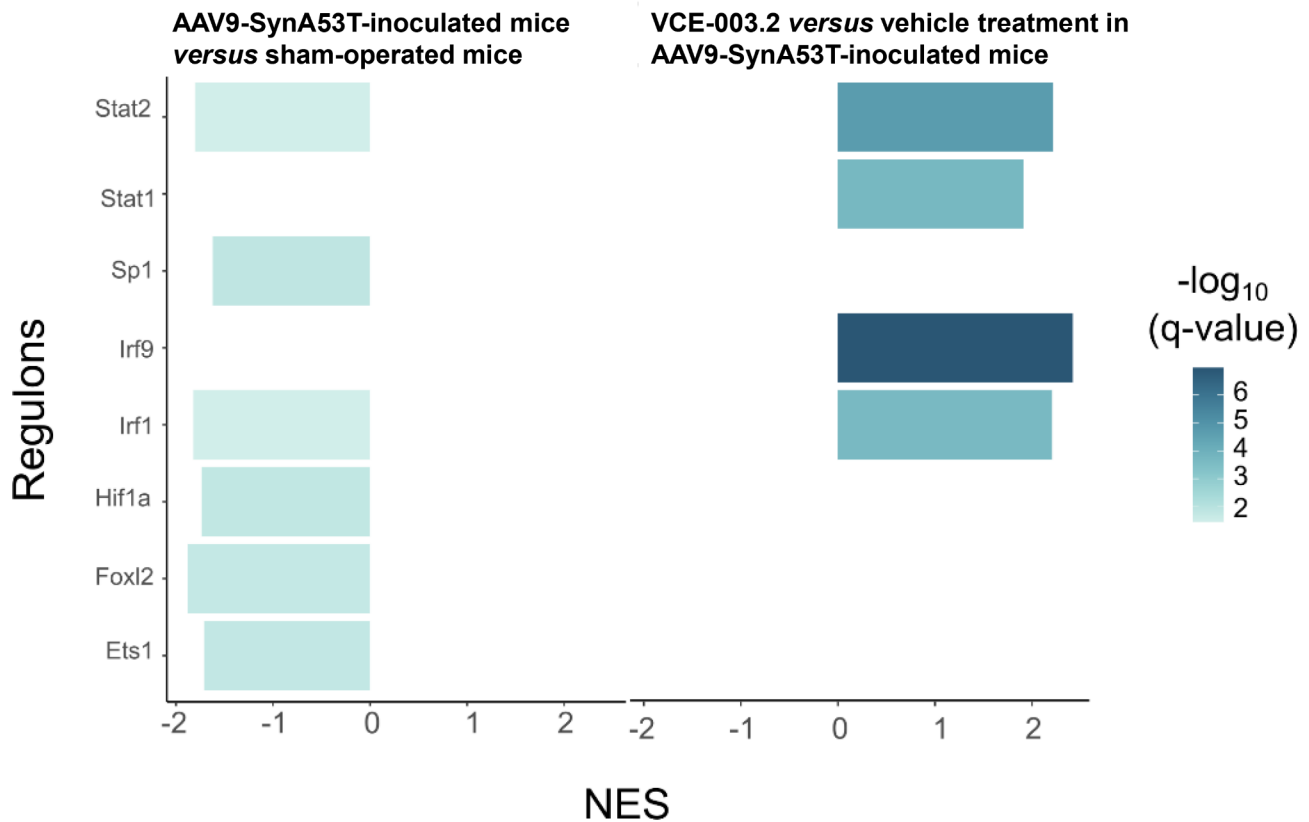


**Fig. 7** Transcription factor enrichment analysis using DoRothEA showing the altered regulons that were significant at  $q$ -value  $< 0.05$ . X-axis shows the directionality and Y-axis the different regulons, with the green color tone reflecting the levels of significance. The significant enrichment for the comparison of AAV9-SynA53T-injected mice versus sham-operated mice, both treated with vehicle, is presented on the left, whereas the one for the comparison of VCE-003.2-treated AAV9-SynA53T-injected mice versus those treated with vehicle is presented on the right

protein-1 (*Sp1*), the tumorigenic factor Forkhead box I2 (*Foxl2*), and others such as Erythroblast transformation specific-1 (*Ets1*) and Hypoxia-inducible factor-1a (*Hif1a*) (Fig. 7 and Supplementary Table 6). Other down-regulated regulon of interest is Interferon regulatory factor-1 (*Irf1*), along with other transcription factors such as Signal transducer and activator of transcription-1 (*Stat1*) and -2 (*Stat2*), the latter also down-regulated (Fig. 7 and Supplementary Table 6). When we compared VCE-003.2-treated AAV9-SynA53T-injected mice with the same animals treated with vehicle, we observed up-regulation for *Stat1*, *Stat2*, *Irf1* and *Irf9* (Fig. 7 and Supplementary Table 6). This suggests that VCE-003.2 may reverse the transcriptomic deficiencies in these factors induced by the neuronal overexpression of mutated  $\alpha$ -synuclein (Fig. 7). Whether this mechanism of action is a key event in the ability of VCE-003.2 to preserve the structure and functionality of the nigrostriatal projection in the basal ganglia, or whether a mere consequence of such neuroprotective effect exerted by VCE-003.2 will require further research. Nevertheless, this finding is a

novel and significant result of our transcriptomic analysis. All raw RNA-Seq data have been uploaded to Array-Express repository to make them available for further analysis (accession number: E-MTAB-13768).

### Discussion

The non-thiophilic CBG quinone derivative VCE-003.2 administered i.p. has been intensely investigated in different experimental models of PD with positive results as a potential disease modifying agent [15, 36]. Its efficacy has also been confirmed through alternative routes of administration (e.g., oral) that may facilitate its further clinical development [12, 15]. However, the in vitro and in vivo models employed in these studies (e.g., LPS-lesioned mice, 6-OHDA-exposed SH-SY5Y cells, 6-OHDA-lesioned mice) fail to reproduce the dysregulation and aggregation of  $\alpha$ -synuclein, a seminal event in PD pathogenesis [16]. In this study, our aim was to assess the potential efficacy of the orally administered VCE-003.2 in a model based on  $\alpha$ -synuclein dysregulation and accumulation, which would contribute to positioning

this cannabinoid derivative for a promising translation to the clinical scenario. Moreover, we have investigated some additional pharmacological characteristics of VCE-003.2 in relation with its ADMET, pharmacokinetics, and secondary pharmacology properties that demonstrate that it counts with high druglikeness and a solid pre-clinical characterization, which reinforce its promising translational potential for this and similar pathological conditions.

To achieve this major objective of our study, we used an experimental model of PD based on the intraparenchymal delivery of AAV9-SynA53T in the SN. This model, previously employed in similar studies evaluating various neuroprotective compounds [18, 66], has demonstrated robustness in recapitulating the expected PD-pathogenic events such as motor defects, elevated levels of  $\alpha$ -synuclein and loss of TH-positive neurons in the SNpc, and the activation of astrocytes and microglial cells. Using this model, we show how the oral administration of VCE-003.2 resulted in preservation of nigral TH-containing neurons, attenuation of glial (microglia and astrocytes) reactivity, and improved performance in the motor tests used. Notably, there was a significant recovery in the CRT and, overall, an increased mobility with respect to mice injected with AAV9-SynA53T. While we anticipated that VCE-003.2 treatment may also reduce  $\alpha$ -synuclein overexpression, given its potential effects by enhancing autophagic and/or lysosomal functions [12], no changes were observed in  $\alpha$ -synuclein levels in the SNpc of mice injected with AAV9-SynA53T after administration of VCE-003.2. Further research is needed to investigate if VCE-003.2 may prevent aggregation leading to the neuroprotection observed.

To shed light in the molecular pathways underlying the biological effects, especially the functional recovery, we performed RNA-Seq analysis of the striatum where we shall observe the consequences of preserving nigrostriatal innervation. We found a substantial transcriptomic change driven by this mutant  $\alpha$ -synuclein overexpression, which fit with some expected changes in gene families encoding for proteins associated, for example, with the oxygen species pathway and the oxidative phosphorylation, features importantly associated to PD [34]. We also observed alterations in pathways associated with autophagy and lysosomal function (e.g., mTORC1 signaling), as well as lipid metabolism (e.g., fatty acid metabolism, adipogenesis), inflammation and the interferon response, all of them previously implicated in the development of PD [2, 5, 42, 50, 58, 68]. Our analysis also included some important PD-related genes such as *Prkn* and *Lrrk2*, which were not altered, and also *Snca* gene which exhibited an important and expected up-regulation derived from the local injection of AAV9-SynA53T into the SN. These findings reinforce the suitability of

the experimental model for preclinical studies in PD in relation with the overexpression of SynA53T, which it is expected that may also reach the caudate-putamen (e.g., through the axons of transfected nigral neurons) despite the AAV9-SynA53T was injected in the SNpc. In fact, the possibility that the AAV9-SynA53T could also reach the caudate-putamen and transfect non-dopaminergic neurons (e.g., striatal projection neurons, striatal interneurons) is an option that cannot be discarded with the present experimental approach, and that may, in part, may explain the singularity in some of changes observed in transcriptomic data (e.g., interferon response). To confirm this possibility will require additional research. Furthermore, we also identified novel groups of genes naïve for PD that would require further analysis to unravel their implication and relevance in the context of PD (Supplementary Tables 2–5). Our transcriptomic analysis also revealed changes in a few genes related to the endocannabinoid system (i.e., *Cnr1*, *Gpr55*, *Faah*) which were exclusively associated with the overexpression of mutated  $\alpha$ -synuclein into the SN, remaining unaltered by the treatment with VCE-003.2. However, what we did observe was a down-regulation of genes involved in interferon signaling pathways driven by  $\alpha$ -synuclein overexpression, the main responsible for anti-viral responses [57]. This effect was reverted by the treatment with VCE-003.2, presumably through the activation of the PPAR- $\gamma$  receptor, according to our previous findings [36]. The PPAR- $\gamma$  receptor is known to be one of the most crucial mediators in the inflammatory response in the brain [9] and also outside the brain (e.g., immune system; Straus and Glass [71]), so it is likely that VCE-003.2 may be active in modulating interferon response. In this case, the pharmacological correction caused by this treatment seems to be orchestrated by *Irf1* and *Irf9* transcription factors, and their coregulators *Stat1* and *Stat2*, responsible for immune and anti-viral responses [57], as their downstream genes were significantly activated after VCE-003.2 treatment. As indicated above, whether this mechanism of action is a key event in the ability of VCE-003.2 to preserve the structure and functionality of the nigrostriatal projection in the basal ganglia, or whether a mere consequence of such neuroprotective effect exerted by VCE-003.2 will require further research. Nevertheless, this finding is a novel and significant result of our transcriptomic analysis. It is also important to remark that the present findings align with existing evidence that highlights an interaction between the signaling pathways of the PPAR- $\gamma$  receptor and type-1 interferons together with their protective effect even observed in an oncological context [25]. When we correlate these upregulated pathways with the diminished expression observed in glial markers, particularly CD68, it may indicate a microglial phenotypic shift characterized by less

reactive microglia and different inflammatory processes [17]. In other words, we hypothesize that the activation of PPAR- $\gamma$  is triggering a protective inflammatory response, which may contribute to the safeguarding of dopaminergic neurons, which we will delve into in future experiments. In support of this idea, our transcriptomic analysis revealed that one of the up-regulated genes by the local overexpression of SynA53T was *Ppargc1b* (logFC=+0.44; FDR=0.04; Supplementary Tables 3 and 4), whereas *Ppargc1a* resulted down-regulated (logFC=-0.42; FDR=0.006; Supplementary Tables 3 and 4). These genes encode for proteins that function as coactivators of PPAR- $\gamma$ , a response triggered in our study by the AAV9-SynA53T-mediated lesion. These results could be interpreted as an endogenous protective response involving PPAR- $\gamma$  signaling upon AAV9-SynA53T inoculation. Treatment with VCE-003.2 may strengthen this signaling pathway through its ability to bind the regulatory site in the PPAR- $\gamma$  receptor, although this will require further research.

Lastly, we also detected a significant enrichment in several regulons of interest in relation with the context (neurodegeneration) of this study, which were down-regulated in vehicle-treated AAV9-SynA53T-injected mice with respect to vehicle-treated sham-operated animals. This was the case of Specificity protein-1 (*Sp1*), which is a zinc finger family transcription factor that can regulate a number of genes that influence cell survival and proliferation [77]. Similar changes were detected for: (i) the tumorigenic factor Forkhead box I2 (*FoxI2*), which has been associated with the control of cellular identity [75]; (ii) Erythroblast transformation specific-1 (*Ets1*), which is expressed at high levels mainly in immune tissues [38], but has been also linked to cellular senescence [76]; and (iii) hypoxia-inducible factor-1a (*Hif1a*), which appears to play an important role in conditions of oxygen deprivation also in chronic neurodegeneration [60].

## Conclusion

Our results extend the neuroprotective potential of VCE-003.2, already described against mitochondrial dysfunction, oxidative stress, glial reactivity and neuroinflammation in PD, to other key pathogenic event in this disease, as  $\alpha$ -synuclein dysregulation and accumulation, and identified some relevant pathways of interest (e.g., interferon signaling) for further research in relation with the molecular mechanisms underlying these beneficial effects. It is true that this potential was particularly evident in relation with behavioral responses and histopathological markers, but the results at the transcriptomic level were not so conclusive, affecting mainly the aforementioned alterations in interferon signaling. This fact opens the door to other regulatory processes such as post-transcriptional modifications or protein activity

modulation that will be investigated in future projects. In any case, these results, together with a favorable absorption, distribution, metabolism, excretion, and toxicology (ADMET) profile, reinforce the preclinical interest of VCE-003.2 towards its future clinical development in PD.

## Abbreviations

AAV9-SynA53T	Adeno-associated viral vector serotype 9 encoding (A53T) $\alpha$ -synuclein
ADMET	Absorption, distribution, metabolism, excretion, and toxicology
BBB	Blood-brain barrier
CB <sub>1</sub> receptor	Cannabinoid type-1 receptor
CB <sub>2</sub> receptor	Cannabinoid type-2 receptor
CBG	Cannabigerol
CPM	Counts per million
CRT	Cylinder rearing test
$\Delta^9$ -THCV	$\Delta^9$ -tetrahydrocannabivarin
DEGs	Differentially expressed genes
EBST	Elevated-body swing test
FAAH	Fatty acid amide hydrolase
FDR	False discovery rate
GFAP	Glial fibrillary acidic protein
LRRK2	Leucine-rich repeat kinase-2
MAGL	Monoacylglycerol lipase
NRF2	Nuclear Factor (Erythroid-derived 2)-related factor 2
6-OHDA	6-hydroxydopamine
PBS	Phosphate-buffered saline
PCA	Principal component analysis
PD	Parkinson's disease
PK	Pharmacokinetics
PPAR- $\gamma$	Peroxisome proliferator-activated receptor- $\gamma$
RNAseq	RNA sequencing analysis
SNpc	Substantia nigra pars compacta
TH	Tyrosine hydroxylase
TRPV <sub>1</sub>	Transient receptor potential vanilloid type-1

## Supplementary Information

The online version contains supplementary material available at <https://doi.org/10.1186/s12993-024-00256-9>.

Supplementary Material 1: Plasmid map for pAAV-synapsin-SynA53T and sequence.

Supplementary Material 2: Chemical structure, in vitro pharmacology data, physicochemical and early ADME properties with relevance for good in vivo performance, and pharmacokinetic profile of VCE-003.2.

Supplementary Material 3: Representative video recordings of the response in the Cylinder Rearing Test (CRT) of vehicle-treated control (sham-operated) adult male mice and unilaterally AAV9-SynA53T-injected adult male mice treated with vehicle or VCE-00.2 (20 mg/kg) given orally. Treatments were daily and prolonged for 2 weeks. Video recordings were obtained at 24 h after the last dose.

Supplementary Material 4: Representative video recordings of the response in the Elevated-Body Swing Test (EBST) of vehicle-treated control (sham-operated) adult male mice and unilaterally AAV9-SynA53T-injected adult male mice treated with vehicle or VCE-00.2 (20 mg/kg) given orally. Treatments were daily and prolonged for 2 weeks. Video recordings were obtained at 24 h after the last dose.

Supplementary Material 5: Computer-aided actimeter (actitrack) analysis of vehicle-treated control (sham-operated) adult male mice and unilaterally AAV9-SynA53T-injected adult male mice treated with vehicle or VCE-00.2 (20 mg/kg) given orally. Treatments were daily and prolonged for 2 weeks. Data corresponded to 24 h after the last dose and were expressed as means  $\pm$  SEM of more than 5 animals per group. They were analyzed by one-way ANOVA followed by the Tukey test (\* $p < 0.05$  versus vehicle-treated sham-operated mice; # $p < 0.05$  versus vehicle-treated AAV9-SynA53T-

injected mice).

Supplementary Material 6: Intensity of the immunostaining for  $\alpha$ -synuclein measured in a selected area of the SNpc of vehicle-treated control (sham-operated) adult male mice and unilaterally AAV9-SynA53T-injected adult male mice treated with vehicle or VCE-00.2 (20 mg/kg) given orally. Treatments were daily and prolonged for 2 weeks. Data corresponded to 24 h after the last dose and were expressed as means  $\pm$  SEM of more than 5 animals *per* group. They were analyzed by one-way ANOVA followed by the Tukey test ( $***p < 0.005$  versus vehicle-treated sham-operated mice). Representative immunostaining images for each experimental group, with indication of the approximate area quantified, are shown in right panels (scale bar = 200  $\mu$ m, and 4x magnification (50  $\mu$ m) in insets).

Supplementary Material 7: Number of TH-positive neurons measured, using a deep-learning dedicated algorithm (Aiforia<sup>®</sup>), in a selected area of the SNpc of vehicle-treated control (sham-operated) adult male mice and unilaterally AAV9-SynA53T-injected adult male mice treated with vehicle or VCE-00.2 (20 mg/kg) given orally. Treatments were daily and prolonged for 2 weeks. Data corresponded to 24 h after the last dose and were expressed as means  $\pm$  SEM of more than 5 animals *per* group. They were analyzed by one-way ANOVA followed by the Tukey test ( $**p < 0.005$  versus vehicle-treated sham-operated mice;  $\#p < 0.05$  versus vehicle-treated AAV9-SynA53T-injected mice).

Supplementary Material 8: Representative GFAP immunostaining images for each experimental group, corresponding to the data presented in the Fig. 4 (scale bar = 200  $\mu$ m).

Supplementary Material 9: Representative CD68 immunostaining images for each experimental group corresponding to higher magnification images selected from those used to generate the data presented in the Fig. 4, with the purpose to identify morphological characteristics (cell body volume, number, thickness and length of cell branches) that may reflect the quiescent or activated states of CD68-labelled cells (scale bar = 100  $\mu$ m).

Supplementary Material 10: Pharmacokinetic parameters of VCE-003.2 in plasma following a single intravenous (IV) (10 mg/kg) and oral (50 mg/kg) dose in CD-1 mice.

Supplementary Material 11: Excel tables showing the data of the RNA-Seq analysis in the striatum of vehicle-treated control (sham-operated) adult male mice and unilaterally AAV9-SynA53T-injected adult male mice treated with vehicle or VCE-00.2 (20 mg/kg) given orally. Treatments were daily and prolonged for 2 weeks. Data corresponded to 24 h after the last dose and were expressed as means  $\pm$  SEM of more than 5 animals *per* group.

#### Data availability

Raw RNA-Seq data have been uploaded to ArrayExpress repository to make them available for further analysis (accession number: E-MTAB-13768). Further information and reasonable request for resources and reagents should be directed to and will be fulfilled by the corresponding authors, Eduardo Muñoz (fi1muble@uco.es) and Javier Fernández-Ruiz (jjfr@med.ucm.es).

#### Ethical approval

All animal experiments were conducted according to local and European rules (directive 2010/63/EU), as well as conformed to ARRIVE guidelines. They were approved by the ethical committees of our university and the regulatory institution (ref. PROEX 201.8/22).

#### Consent for publication

Not applicable.

#### Competing interests

The authors declare no competing interests.

#### Author details

<sup>1</sup>Departamento de Bioquímica y Biología Molecular, Facultad de Medicina, Instituto Universitario de Investigación en Neuroquímica, Universidad Complutense, Madrid, Spain

<sup>2</sup>Centro de Investigación Biomédica en Red de Enfermedades Neurodegenerativas (CIBERNED), Madrid, Spain

<sup>3</sup>Instituto Ramón y Cajal de Investigación Sanitaria (IRYCIS), Madrid, Spain

<sup>4</sup>Emerald Health Pharmaceuticals, San Diego, USA

<sup>5</sup>Instituto Maimónides de Investigación Biomédica de Córdoba (IMIBIC), Córdoba, Spain

<sup>6</sup>Departamento de Biología Celular, Fisiología e Inmunología, Universidad de Córdoba, Córdoba, Spain

<sup>7</sup>Hospital Universitario Reina Sofía, Córdoba, Spain

<sup>8</sup>Instituto de Investigaciones Biomédicas Sols-Morreales (IIBSM), UAM-CSIC, Madrid, Spain

<sup>9</sup>Departamento de Bioquímica, Facultad de Medicina, Universidad Autónoma de Madrid (UAM), Madrid, Spain

<sup>10</sup>Instituto de Investigación del Hospital Universitario de La Paz (IdiPAZ), Madrid, Spain

<sup>11</sup>Institute Teófilo Hernando for Drug Discovery, Universidad Autónoma de Madrid, Madrid, Spain

<sup>12</sup>CNS Gene Therapy Department, Center for Applied Medical Research (CIMA), Universidad de Navarra, Pamplona, Spain

Received: 20 May 2024 / Accepted: 18 October 2024

Published online: 01 November 2024

#### Acknowledgements

Authors are indebted to Yolanda García-Movellán for administrative assistance and to CAI-Animalario, Complutense University for animal housing and care.

#### Author contributions

J.F.-R. wrote the different manuscript drafts, which were revised and approved by all authors. J.F.-R. and E.M. designed, coordinated and supervised the study, and were involved in funding acquisition. S.B., I.L.-B., J.L.L. and S.R.-C. were involved in the development of the mouse model. S.B., S.R.-C. and J.Ch. carried out the behavioural and histopathological analyses, whereas E.N., M.G.-R. and C.N. conducted the transcriptomic analysis. C.N. and E.M. coordinated the VCE-003.2 synthesis and its pharmacological characterization. J.F.-R. and EN carried out all statistical analysis of the data.

#### Funding

This work has been supported by grants from CIBERNED (CB06/05/0089 to JF-R), MICINN (PID2021-128906OB-I00 to JF-R, PID2022-139936OA-I00 to EN and PID2022-137065OB-I00 to ILB) with FEDER funds and Michael J. Fox Foundation (MJFF-022552 to JF-R). These agencies had no further role in study design, the collection, analysis, and interpretation of data, in the writing of the report, or in the decision to submit the paper for publication. Sonia Burgaz was a predoctoral fellow supported by the Complutense University, whereas Santiago Rodríguez-Carreiro was supported by the Ministry of University (FPU Programme).

#### References

1. Aguales J, Paraíso-Luna J, Palomares B, Bajo-Grañeras R, Navarrete C, Ruiz-Calvo A, García-Rincón D, García-Taboada E, Guzmán M, Muñoz E, Galve-Roperh I. Oral administration of the cannabigerol derivative VCE-003.2 promotes subventricular zone neurogenesis and protects against mutant huntingtin-induced neurodegeneration. *Translational Neurodegeneration*. 2019;8:9.
2. Anand S, Azam Ansari M, Kumaraswamy Sukrutha S, Alomary MN, Anwar Khan A, Elderderly AY. Resolvins lipid mediators: potential therapeutic targets in Alzheimer and Parkinson disease. *Neuroscience*. 2022;507:139–48.
3. Antonazzo M, Botta M, Bengoetxea H, Ruiz-Ortega JA, Morera-Herreras T. Therapeutic potential of cannabinoids as neuroprotective agents for damaged cells conducting to movement disorders. *Int Rev Neurobiol*. 2019;146:229–57.
4. Aymerich MS, Aso E, Abellanas MA, Tolon RM, Ramos JA, Ferrer I, Romero J, Fernández-Ruiz J. Cannabinoid pharmacology/therapeutics in chronic degenerative disorders affecting the central nervous system. *Biochem Pharmacol*. 2018;157:67–84.
5. Basurco L, Abellanas MA, Ayerra L, Conde E, Vinuesa-Gavilanes R, Luquin E, Vales A, Vilas A, Martín-Uriz PS, Tamayo I, Alonso MM, Hernaez M, Gonzalez-Aseguinolaza G, Clavero P, Mengual E, Arrasate M, Hervás-Stubbbs S, Aymerich MS. Microglia and astrocyte activation is region-dependent in the  $\alpha$ -synuclein mouse model of Parkinson's disease. *Glia*. 2022;71:571–87.

- 6 Bajaj S, Jain S, Vyas P, Bawa S, Vohora D. The role of endocannabinoid pathway in the neuropathology of Alzheimer's disease: can the inhibitors of MAGL and FAAH prove to be potential therapeutic targets against the cognitive impairment associated with Alzheimer's disease? *Brain Res Bull.* 2021;174:305–22.
- 7 Baul HS, Manikandan C, Sen D. Cannabinoid receptor as a potential therapeutic target for Parkinson's disease. *Brain Res Bull.* 2019;146:244–52.
- 8 Bentea E, Van der Perren A, Van Liefferinge J, El Arfani A, Albertini G, Demuyser T, Merckx E, Michotte Y, Smolders I, Baekelandt V, Massie A. Nigral proteasome inhibition in mice leads to motor and non-motor deficits and increased expression of Ser129 phosphorylated  $\alpha$ -synuclein. *Front Behav Neurosci.* 2015;9:68.
- 9 Bernardo A, Minghetti L. PPAR- $\gamma$  agonists as regulators of microglial activation and brain inflammation. *Curr Pharm Design.* 2006;12:93–109.
- 10 Björklund A, Mattsson B. (2024) The AAV- $\alpha$ -synuclein model of Parkinson's disease: An update. *J Parkinsons Dis.* in press.
- 11 Borlongan CV, Sanberg PR. Elevated body swing test: a new behavioral parameter for rats with 6-hydroxydopamine-induced hemiparkinsonism. *J Neurosci.* 1995;15:5372–8.
- 12 Burgaz S, García C, Gómez-Cañas M, Muñoz E, Fernández-Ruiz J. Development of an oral treatment with the PPAR- $\gamma$ -acting cannabinoid VCE-003.2 against the inflammation-driven neuronal deterioration in experimental Parkinson's disease. *Molecules.* 2019;24:2702.
- 13 Burgaz S, García C, Gómez-Cañas M, Rolland A, Muñoz E, Fernández-Ruiz J. Neuroprotection with the cannabidiol quinone derivative VCE-004.8 (EHP-101) against 6-hydroxydopamine in cell and murine models of Parkinson's disease. *Molecules.* 2021a;26:3245.
- 14 Burgaz S, García C, Gonzalo-Consuegra C, Gómez-Almería M, Ruiz-Pino F, Unciti JD, Gómez-Cañas M, Alcalde J, Morales P, Jagerovic N, Rodríguez-Cueto C, de Lago E, Muñoz E, Fernández-Ruiz J. Preclinical investigation in neuroprotective effects of the GPR55 ligand VCE-006.1 in experimental models of Parkinson's disease and amyotrophic lateral sclerosis. *Molecules.* 2021b;26:7643.
- 15 Burgaz S, García C, Gómez-Cañas M, Navarrete C, García-Martín A, Rolland A, Del Río C, Casarejos MJ, Muñoz E, Gonzalo-Consuegra C, Muñoz E, Fernández-Ruiz J. Neuroprotection with the cannabigerol quinone derivative VCE-003.2 and its analogs CBGA-Q and CBGA-Q-Salt in Parkinson's disease using 6-hydroxydopamine-lesioned mice. *Mol Cell Neurosci.* 2021c;110:103583.
- 16 Calabresi P, Mechelli A, Natale G, Volpicelli-Daley L, Di Lazzaro G, Ghiglieri V.  $\alpha$ -Synuclein in Parkinson's disease and other synucleinopathies: from overt neurodegeneration back to early synaptic dysfunction. *Cell Death Dis.* 2023;14:176.
- 17 Carta AR, Pisanu A. Modulating microglia activity with PPAR- $\gamma$  agonists: a promising therapy for Parkinson's disease? *Neurotox Res.* 2013;23:112–23.
- 18 Castro-Sánchez S, García-Yagüe AJ, López-Royo T, Casarejos MJ, Lanciego JL, Lastres-Becker I. Cx3cr1-deficiency exacerbates  $\alpha$ -synuclein-A53T induced neuroinflammation and neurodegeneration in a mouse model of Parkinson's disease. *Glia.* 2018;66:1752–62.
- 19 Celorrio M, Rojo-Bustamante E, Fernández-Suárez D, Sáez E, Estella-Hermoso de Mendoza A, Müller CE, Ramírez MJ, Oyarzábal J, Franco R, Aymerich MS. GPR55: a therapeutic target for Parkinson's disease? *Neuropharmacology.* 2017;125:319–32.
- 20 Chen C. Inhibiting degradation of 2-arachidonoylglycerol as a therapeutic strategy for neurodegenerative diseases. *Pharmacol Ther.* 2023;244:108394.
- 21 Chocarro J, Rico AJ, Ariznabarreta G, Roda E, Honrubia A, Collantes M, Peñuelas I, Vázquez A, Rodríguez-Pérez AI, Labandeira-García JL, Vila M, Lanciego JL. Neuromelanin accumulation drives endogenous synucleinopathy in non-human primates. *Brain.* 2023;146:5000–14.
- 22 Chung YC, Bok E, Huh SH, Park JY, Yoon SH, Kim SR, Kim YS, Maeng S, Park SH, Jin BK. Cannabinoid receptor type 1 protects nigrostriatal dopaminergic neurons against MPTP neurotoxicity by inhibiting microglial activation. *J Immunol.* 2011;187:6508–17.
- 23 Coles M, Steiner-Lim GZ, Karl T. Therapeutic properties of multi-cannabinoid treatment strategies for Alzheimer's disease. *Front Neurosci.* 2022;16:962922.
- 24 Díaz-Alonso J, Paraíso-Luna J, Navarrete C, Del Río C, Cantarero I, Palomares B, Aguales J, Fernández-Ruiz J, Bellido ML, Pollastro F, Appendino G, Calzado MA, Galve-Roperh I, Muñoz E. VCE-003.2, a novel cannabigerol derivative, enhances neuronal progenitor cell survival and alleviates symptomatology in murine models of Huntington's disease. *Sci Rep.* 2016;6:29789.
- 25 Dicitore A, Caraglia M, Gaudenzi G, Manfredi G, Amato B, Mari D, Persani L, Arra C, Vitale G. Type I interferon-mediated pathway interacts with peroxisome proliferator activated receptor- $\gamma$  (PPAR- $\gamma$ ): at the cross-road of pancreatic cancer cell proliferation. *Biochim Biophys Acta.* 2014;1845:42–52.
- 26 Espadas I, Keifman E, Palomo-Garo C, Burgaz S, García C, Fernández-Ruiz J, Moratalla R. Beneficial effects of the phytocannabinoid  $\Delta^9$ -THCV in L-DOPA-induced dyskinesia in Parkinson's disease. *Neurobiol Dis.* 2020;141:104892.
- 27 Fernández-Moncada I, Eraso-Pichot A, Dalla Tor T, Fortunato-Marsol B, Marsicano G. An enquiry to the role of CB1 receptors in neurodegeneration. *Neurobiol Dis.* 2023;184:106235.
- 28 Fernández-Ruiz J. The endocannabinoid system as a target for the treatment of motor dysfunction. *Br J Pharmacol.* 2009;156:1029–40.
- 29 Fernández-Ruiz J, Moreno-Martet M, Rodríguez-Cueto C, Palomo-Garo C, Gómez-Cañas M, Valdeolivas S, Guaza C, Romero J, Guzmán M, Mechoulam R, Ramos JA. Prospects for cannabinoid therapies in basal ganglia disorders. *Br J Pharmacol.* 2011;163:1365–78.
- 30 Fernández-Ruiz J, Moro MA, Martínez-Orgado J. Cannabinoids in neurodegenerative disorders and stroke/brain trauma: from preclinical models to clinical applications. *Neurotherapeutics.* 2015;12:793–806.
- 31 Fernández-Ruiz J. The biomedical challenge of neurodegenerative disorders: an opportunity for cannabinoid-based therapies to improve on the poor current therapeutic outcomes. *Br J Pharmacol.* 2019;176:1370–83.
- 32 Ferrisi R, Ceni C, Bertini S, Macchia M, Manera C, Gado F. Medicinal chemistry approach, pharmacology and neuroprotective benefits of CB<sub>2</sub>R modulators in neurodegenerative diseases. *Pharmacol Res.* 2021;170:105607.
- 33 Fleming SM, Ekhtor OR, Ghisays V. Assessment of sensorimotor function in mouse models of Parkinson's disease. *J Visualized Experiments.* 2013;76:50303.
- 34 Ganjam GK, Bolte K, Matschke LA, Neitemeier S, Dolga AM, Höllner M, Höglinger GU, Adamczyk A, Decher N, Oertel WH, Culumsee C. Mitochondrial damage by  $\alpha$ -synuclein causes cell death in human dopaminergic neurons. *Cell Death Dis.* 2019;10:865.
- 35 García C, Palomo-Garo C, García-Arencibia M, Ramos JA, Pertwee RG, Fernández-Ruiz J. Symptom-relieving and neuroprotective effects of the phytocannabinoid  $\Delta^8$ -THCV in animal models of Parkinson's disease. *Br J Pharmacol.* 2011;163:1495–506.
- 36 García C, Gómez-Cañas M, Burgaz S, Palomares B, Gómez-Gálvez Y, Palomo-Garo C, Campo S, Ferrer-Hernández J, Pavicic C, Navarrete C, Bellido ML, García-Arencibia M, Pazos MR, Muñoz E, Fernández-Ruiz J. Benefits of VCE-003.2, a cannabigerol quinone derivative, against inflammation-driven neuronal deterioration in experimental Parkinson's disease: possible involvement of different binding sites at the PPAR $\gamma$  receptor. *J Neuroinflamm.* 2018;15:19.
- 37 García-Alonso L, Holland CH, Ibrahim MM, Turei D, Saez-Rodríguez J. Benchmark and integration of resources for the estimation of human transcription factor activities. *Genome Res.* 2019;29:1363–75.
- 38 Garrett-Sinha LA. An update on the roles of transcription factor Ets1 in autoimmune diseases. *WIREs Mech Dis.* 2023;15:e1627.
- 39 Gómez-Gálvez Y, Palomo-Garo C, Fernández-Ruiz J, García C. Potential of the cannabinoid CB<sub>2</sub> receptor as a pharmacological target against inflammation in Parkinson's disease. *Progress Neuropsychopharmacol Biol Psychiatry.* 2016;64:200–8.
- 40 Gugliandolo A, Pollastro F, Grassi G, Bramanti P, Mazzon E. (2018) In Vitro model of neuroinflammation: efficacy of cannabigerol, a non-psychoactive cannabinoid. *International Journal of Molecular Sciences* 19, 1992.
- 41 Holland CH, Szalai B, Saez-Rodríguez J. Transfer of regulatory knowledge from human to mouse for functional genomics analysis. *Biochim Biophys Acta.* 2020;1863:194431.
- 42 Iba M, McDevitt RA, Kim C, Roy R, Sarantopoulou D, Tommer E, Siegars B, Sallin M, Kwon S, Sen JM, Sen R, Maslah E. Aging exacerbates the brain inflammatory micro-environment contributing to  $\alpha$ -synuclein pathology and functional deficits in a mouse model of DLB/PD. *Mol Neurodegeneration.* 2022;17:60.
- 43 Jain V, Behl T, Sehgal A, Singh S, Sharma N, Makeen HA, Albratty M, Meraya AM, Najmi A. Therapeutic molecular insights into the active engagement of cannabinoids in the therapy of Parkinson's disease: a novel and futuristic approach. *Neurotox Res.* 2023;41:85–102.
- 44 Javed H, Azimullah S, Haque ME, Ojha SK. Cannabinoid type 2 (CB<sub>2</sub>) receptors activation protects against oxidative stress and neuroinflammation associated dopaminergic neurodegeneration in rotenone model of Parkinson's disease. *Front Neurosci.* 2016;10:321.
- 45 Kelly R, Bemelmans AP, Joséphine C, Brouillet E, McKernan DP, Dowd E. Time-course of alterations in the endocannabinoid system after viral-mediated overexpression of  $\alpha$ -synuclein in the rat brain. *Molecules.* 2022;27:507.
- 46 Kelsey JE, Harris O, Cassin J. The CB<sub>1</sub> antagonist rimonabant is adjunctively therapeutic as well as monotherapeutic in an animal model of Parkinson's disease. *Behav Brain Res.* 2009;203:304–7.

- 47 Kim D, Langmead B, Salzberg SL. HISAT: a fast spliced aligner with low memory requirements. *Nat Methods*. 2015;12:357–60.
- 48 Ko WKD, Bezdard E. Experimental animal models of Parkinson's disease: a transition from assessing symptomatology to  $\alpha$ -synuclein targeted disease modification. *Exp Neurol*. 2017;298:172–9.
- 49 Korotkevich G, Sukhov V, Budin N, Shpak B, Artyomov MN, Sergushichev A. Fast gene set enrichment analysis. *BioRxiv* (doi). 2021. <https://doi.org/10.1101/060012>.
- 50 Kuo SH, Tasset I, Cheng MM, Diaz A, Pan MK, Lieberman OJ, Hutten SJ, Alcalay RN, Kim S, Ximénez-Embún P, Fan L, Kim D, Ko HS, Yacoubian T, Kanter E, Liu L, Tang G, Muñoz J, Sardi SP, Li A, Gan L, Cuervo AM, Sulzer D. Mutant glucocerebrosidase impairs  $\alpha$ -synuclein degradation by blockade of chaperone-mediated autophagy. *Sci Adv*. 2022;8:eabm6393.
- 51 Lastres-Becker I, Molina-Holgado F, Ramos JA, Mechoulam R, Fernández-Ruiz J. Cannabinoids provide neuroprotection against 6-hydroxydopamine toxicity in vivo and in vitro: relevance to Parkinson's disease. *Neurobiol Dis*. 2005;19:96–107.
- 52 Lastres-Becker I, Ulusoy A, Innamorato NG, Sahin G, Rábano A, Kirik D, Cuadrado A.  $\alpha$ -Synuclein expression and Nrf2 deficiency cooperate to aggravate protein aggregation, neuronal death and inflammation in early-stage Parkinson's disease. *Hum Mol Genet*. 2012;21:3173–92.
- 53 Li B, Dewey CN. RSEM: accurate transcript quantification from RNA-Seq data with or without a reference genome. *BMC Bioinformatics*. 2011;12:323.
- 54 Liao Y, Smyth GK, Shi W. FeatureCounts: an efficient general purpose program for assigning sequence reads to genomic features. *Bioinformatics*. 2014;30:923–30.
- 55 Lins BR, Anyaegbu CC, Hellewell SC, Papini M, McGonigle T, De Prato L, Shales M, Fitzgerald M. Cannabinoids in traumatic brain injury and related neuropathologies: preclinical and clinical research on endogenous, plant-derived, and synthetic compounds. *J Neuroinflamm*. 2023;20:77.
- 56 Marmion DJ, Kordower JH.  $\alpha$ -Synuclein nonhuman primate models of Parkinson's disease. *J Neural Transm*. 2018;125:385–400.
- 57 Muhuri M, Maeda Y, Ma H, Ram S, Fitzgerald KA, Tai PW, Gao G. (2021) Overcoming innate immune barriers that impede AAV gene therapy vectors. *J Clin Invest* 131, e143780.
- 58 Nascimento AC, Erustes AG, Reckziegel P, Bincioletto C, Ureshino RP, Pereira G, Smaili SS.  $\alpha$ -Synuclein overexpression induces lysosomal dysfunction and autophagy impairment in human neuroblastoma SH-SY5Y. *Neurochem Res*. 2020;45:2749–61.
- 59 Navarro E, Udine E, de Paiva Lopes K, Parks M, Riboldi G, Schilder BM, Humphrey J, Snijders GJL, Vialle RA, Zhuang M, Sikder T, Argyrou C, Allan A, Chao MJ, Farrell K, Henderson B, Simon S, Raymond D, Elango S, Ortega RA, Shanker V, Swan M, Zhu CW, Ramdhani R, Walker RH, Tse W, Sano M, Pereira AC, Ahfeldt T, Goate AM, Bressman S, Cray JF, de Witte L, Frucht S, Saunders-Pullman R, Raj T. Dysregulation of mitochondrial and proteolysosomal genes in Parkinson's disease myeloid cells. *Nat Aging*. 2021;1:850–63.
- 60 Ogunshola OO, Antoniou X. Contribution of hypoxia to Alzheimer's disease: is HIF-1 $\alpha$  a mediator of neurodegeneration? *Cell Mol Life Sci*. 2009;66:3555–63.
- 61 Penttinen AM, Parkkinen I, Blom S, Kopra J, Andressoo JO, Pitkänen K, Voutilainen MH, Saarna M, Airavaara M. Implementation of deep neural networks to count dopamine neurons in substantia nigra. *Eur J Neurosci*. 2018;48:2354–61.
- 62 Pérez-Rial S, García-Gutiérrez MS, Molina JA, Pérez-Nievas BG, Ledent C, Leiva C, Leza JC, Manzanares J. Increased vulnerability to 6-hydroxydopamine lesion and reduced development of dyskinesias in mice lacking CB1 cannabinoid receptors. *Neurobiol Aging*. 2011;32:631–45.
- 63 Rico AJ, Corcho A, Chocarro J, Ariznabarreta G, Roda E, Honrubia A, Arnaiz P, Lanciego JL. Development and characterization of a non-human primate model of disseminated synucleinopathy. *Front Neuroanat*. 2024;18:1355940.
- 64 Ritchie ME, Phipson B, Wu D, Hu Y, Law CW, Shi W, Smyth GK. (2015) Limma powers differential expression analyses for RNA-sequencing and microarray studies. *Nucleic Acids Res* 43, e47.
- 65 Rodríguez-Cueto C, García-Toscano L, Santos-García I, Gómez-Almería M, Gonzalo-Consuegra C, Espejo-Porras F, Fernández-Ruiz J, de Lago E. Targeting the CB<sub>2</sub> receptor and other endocannabinoid elements to delay disease progression in amyotrophic lateral sclerosis. *Br J Pharmacol*. 2021;178:1373–87.
- 66 Rodríguez-Pérez AI, Sucunza D, Pedrosa MA, Garrido-Gil P, Kulisevsky J, Lanciego JL, Labandeira-García JL. Angiotensin type 1 receptor antagonists protect against  $\alpha$ -synuclein-induced neuroinflammation and dopaminergic neuron death. *Neurotherapeutics*. 2018;15:1063–81.
- 67 Sañudo-Peña MC, Patrick SL, Khen S, Patrick RL, Tsou K, Walker JM. Cannabinoid effects in basal ganglia in a rat model of Parkinson's disease. *Neurosci Lett*. 1998;248:171–4.
- 68 Siddiqui T, Bhatt LK. (2023) Emerging autophagic endo-lysosomal targets in the management of Parkinson's disease. *Rev Neurol (Paris)*, in press.
- 69 Spillantini MG, Schmidt ML, Lee VM, Trojanowski JQ, Jakes R, Goedert M. Alpha-synuclein in Lewy bodies. *Nature*. 1997;388:839–40.
- 70 Stone NL, Murphy AJ, England TJ, O'Sullivan SE. A systematic review of minor phytocannabinoids with promising neuroprotective potential. *Br J Pharmacol*. 2020;177:4330–52.
- 71 Straus DS, Glass CK. Anti-inflammatory actions of PPAR ligands: new insights on cellular and molecular mechanisms. *Trends Immunol*. 2007;28:551–8.
- 72 Subramanian A, Tamayo P, Mootha VK, Mukherjee S, Ebert BL, Gillette MA, Paulovich A, Pomeroy SL, Golub TR, Lander ES, Mesirov JP. Gene set enrichment analysis: a knowledge-based approach for interpreting genome-wide expression profiles. *Proc Natl Acad Sci USA*. 2005;102:15545–50.
- 73 Tambe SM, Mali S, Amin PD, Oliveira M. Neuroprotective potential of cannabidiol: molecular mechanisms and clinical implications. *J Integr Med*. 2023;21:236–44.
- 74 Wang G, Ma W, Du J.  $\beta$ -Caryophyllene (BCP) ameliorates MPP<sup>+</sup> induced cytotoxicity. *Biomed Pharmacother*. 2018;103:1086–91.
- 75 Wijchers PJ, Hoekman MF, Burbach JP, Smidt MP. Cloning and analysis of the murine Foxi2 transcription factor. *Biochim Biophys Acta*. 2005;1731:133–8.
- 76 Xiao FH, Yu Q, Deng ZL, Yang K, Ye Y, Ge MX, Yan D, Wang HT, Chen XQ, Yang LQ, Yang BY, Lin R, Zhang W, Yang XL, Dong L, He Y, Zhou J, Cai WW, Li J, Kong QP. (2022) ETS1 acts as a regulator of human healthy aging via decreasing ribosomal activity. *Science Advances* 8, eabf2017.
- 77 Yu Q, Liu W, Chen Z, Zhang M. Specificity protein 1: a protein with a two-sided role in ischemic stroke. *Front Cell Neurosci*. 2021;15:757670.
- 78 Zamanian MY, Terefe EM, Taheri N, Kujawska M, Tork YJ, Abdelbasset WK, Shoukat S, Opulencia MJC, Heidari M, Alesaeidi S. Neuroprotective and anti-inflammatory effects of pioglitazone on Parkinson's disease: a comprehensive narrative review of clinical and experimental findings. *CNS Neurol Disorders Drug Targets*. 2023;22:1453–61.

## Publisher's note

Springer Nature remains neutral with regard to jurisdictional claims in published maps and institutional affiliations.